21st IAEA Fusion Energy Conference
Chengdu, China, 16 - 21 October, 2006

IAEA-CN-149/ TH/P2-21

Multi-Scale-Nonlinear Interactions among Micro-turbulence, Magnetic Islands, and Zonal Flows

A. Ishizawa et al.

NIFS-859 Oct. 2006

Multi-Scale-Nonlinear Interactions among Micro-Turbulence, Magnetic Islands, and Zonal Flows

A. Ishizawa 1), N. Nakajima 1), M. Okamoto 1), and J. J. Ramos 2)

1) National Institute for Fusion Science, Toki, Gifu, 509-5929, Japan
2) Massachusetts Institute of Technology, Cambridge, Massachusetts, 02193, U.S.A.

e-mail contact of main author : ishizawa@nifs.ac.jp

Abstract. We investigate multi-scale-nonlinear interactions among micro-instabilities, macro-scale tearing instabilities and zonal flows, by solving reduced two-fluid equations numerically. We find that the nonlinear interactions of these instabilities trigger macro-scale MHD activity after an equilibrium is formed by a balance between the micro-turbulence and zonal flow. This MHD activity breaks magnetic surfaces then this breaking spreads the micro-turbulence over the plasma. These multi-scale-nonlinear interactions can explain the evolution of fluctuation observed in torus plasma experiments because micro-turbulence and MHD instabilities usually appear in the plasma at the same time, in spite of the fact that effects of micro-turbulence and MHD instabilities on plasma confinement have been investigated separately. For instance, MHD activities are observed in reversed shear tokamak plasmas with a transport barrier related to zonal flows and micro-turbulence, and micro-turbulence is observed in Large Helical Device plasmas that usually exhibit MHD activities.

1. Introduction

Effects of micro-turbulence and MHD instabilities on plasma confinement have been investigated separately, but these instabilities usually appear in the plasma at the same time and interact each other as shown in Fig. 1. For instance, MHD activities are observed in reversed shear plasmas with a transport barrier related to zonal flows and micro-turbulence[1], and micro-turbulence is observed in Large Helical Device plasmas that usually exhibit MHD activities[2]. Our goal is to understand the mechanism of the macro-scale MHD activities and their effects on the disruption in the reversed shear plasmas based on the analysis of multi-scale-nonlinear interactions among the micro-turbulence, macro-scale MHD and zonal flows.

A typical multi-scale interaction in magnetic confinement is a mutual interaction between zonal flow and micro-turbulence[3]. This interaction is responsible to evaluate anomalous transport due to the micro-turbulence[4]. Another typical example is the interaction of macro-MHD with turbulence [5, 6, 7, 8, 9, 10]. This nonlinear mode coupling can be described by a negative eddy viscosity[11, 12] or by an anomalous resistivity.

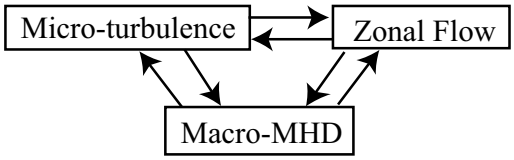

FIG. 1: *Multi-scale-nonlinear interactions among micro-turbulence, macro-scale MHD, and zonal flows*

In this paper, we investigate multi-scale-nonlinear interactions among micro-instabilities, macro-scale tearing instabilities and zonal flows, by solving reduced two-fluid equations numerically. We demonstrate numerically that the nonlinear interactions of these instabilities trigger macro-scale MHD activity after an equilibrium is established by a balance between micro-turbulence and zonal flow. This MHD activity spreads the micro-turbulence over the plasma because it breaks magnetic surfaces. The new mechanism of macro-MHD activity can explain the evolution of fluctuation observed in torus plasma experiments because micro-turbulence and MHD instabilities usually appear in the plasma at the same time.

2. Equations and linear instabilities

We developed a new simulation code solving a reduced set of two-fluid equations that extends the standard reduced two-fluid equations[13], by including temperature gradient effects[14, 15, 16]. We carry out three-dimensional simulations with this simulation code. By solving this set of equations, we can describe the nonlinear evolution of tearing modes, interchange modes, ballooning modes and ion temperature gradient modes. The equations are

$$n_{eq}\frac{dQ}{dt} = -\nabla_{\parallel}J - K[p] + \nabla_{\perp}\cdot[\nabla_{\perp}\Phi, p_i] + \mu_Q\nabla_{\perp}^2 Q, \tag{1}$$

$$\frac{dn}{dt} = -n_{eq}\nabla_{\parallel}v_{e\parallel} + K[n_{eq}\Phi - p_e] + \mu_n\nabla_{\perp}^2 n, \tag{2}$$

$$n_{eq}\frac{dv_{\parallel}}{dt} = -\nabla_{\parallel}p + \mu_v\nabla_{\perp}^2 v_{\parallel}, \tag{3}$$

$$\beta\frac{\partial\psi}{\partial t} = -\nabla_{\parallel}\Phi + \nabla_{\parallel}p_e + \eta_L v_{e\parallel} + \eta J, \tag{4}$$

$$\frac{dT_i}{dt} = -(\Gamma-1)(T_{eq}\nabla_{\parallel}v_{\parallel} + \kappa_L T_i) - T_{eq}K[(\Gamma-1)(\Phi + T_i + T_{eq}/n_{eq}n) + \Gamma T_i] + \mu_T\nabla_{\perp}^2 T_i, \tag{5}$$

where $df/dt = \partial f/\partial t + \tilde{a}[\Phi, f]$, $\nabla_{\parallel}f = \epsilon\partial f/\partial\zeta - \beta\tilde{a}[\psi, f]$, $K[f] = 2\epsilon[r\cos\theta, f]$, $J = \nabla_{\perp}^2\psi$, $Q = \nabla_{\perp}^2\Phi$, $\psi = \psi_{eq} + \tilde{\psi}/\tilde{a}$, $\Phi = \tilde{\Phi}/\tilde{a}$, $n = n_{eq} + \tilde{n}/\tilde{a}$, $T_i = T_{eq} + \tilde{T}_i/\tilde{a}$, $T_e = \tau T_{eq}$, $p_i = n_{eq}T_{eq} + T_{eq}\tilde{n}/\tilde{a} + n_{eq}\tilde{T}_i/\tilde{a}$, $p_e = \tau n_{eq}T_{eq} + \tau T_{eq}\tilde{n}/\tilde{a}$, $p = p_i + p_e$, $v_{e\parallel} = v_{\parallel} + J/n_{eq}$, $\tilde{a} = a/\rho_i$, $\eta_L = \sqrt{\frac{\pi}{2}\tau\frac{m_e}{m_i}}|\nabla_{\parallel}|$, $\kappa_L = (\Gamma-1)\sqrt{\frac{8T_{eq}}{\tau}}|\nabla_{\parallel}|$, ψ is the flux function and Φ is the electric potential. The normalizations are $(tv_{ti}/a, r/\rho_i, \rho_i\nabla_{\perp}, a\nabla_{\parallel}, e\Phi/T_0, \psi/\beta B_0\rho_i, n/n_0, T/T_0, v_{\parallel}/v_{ti}) \to (t, r, \nabla_{\perp}, \nabla_{\parallel}, \Phi, \psi, n, T, v_{\parallel})$. The $r\theta$-plane is normal to the toroidal field B_T. The constants η and μ_a denote the normalized resistivity and the normalized viscosity, respectively. In the numerical calculation we set $\mu_a = m^4 10^{-7}$ and $\eta = 4\times10^{-4}$ which corresponds to $S = 1.6\times10^6$. As boundary conditions the plasma is assumed to be surrounded by a perfectly conducting wall.

Let us briefly describe the algorithm of our simulation code. The time advancement is made with the predictor-corrector method and the radial derivative is approximated by the finite-difference method. The Fourier decomposition is used in the poloidal and toroidal directions as $\psi = \psi_{eq}(r) + \sum_{m,n}\psi_{m,n}(r,t)\exp(im\theta - in\zeta)$ and $\Phi = \sum_{m,n}\Phi_{m,n}(r,t)\exp(im\theta - in\zeta)$, where m and n are poloidal and toroidal mode numbers. In the numerical calculations we employ 256 poloidal modes, 128 toroidal modes, and 256 uniform grid points in the radial direction.

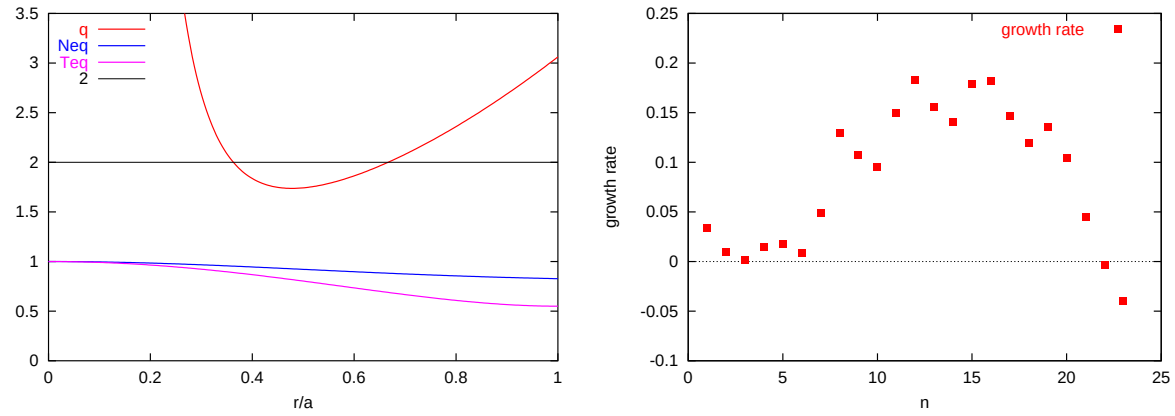

FIG. 2: *Equilibrium profiles and growth rate of linear instabilities.*

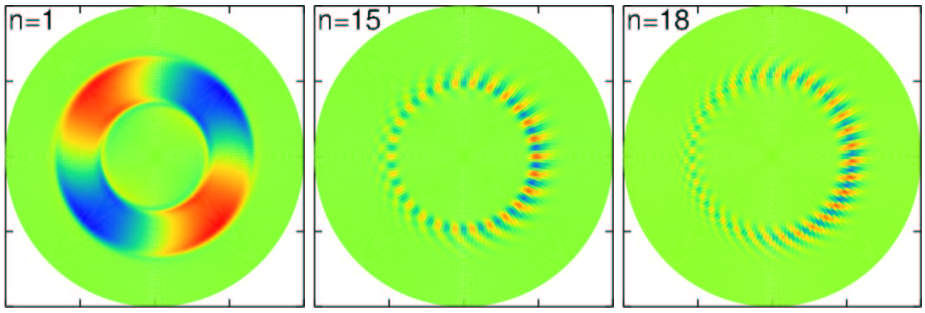

FIG. 3: *The electric potential profile of eigen function on a poloidal section for instabilities:* $n = 1$ *double tearing mode,* $n = 15$ *and* 18 *micro-instabilities.*

We checked the validity of our numerical simulation code by comparing with results by other simulation codes. The Poisson-bracket term is compared with the corresponding term of the code presented in Ref.[17]. The toroidal curvature term is compared with the corresponding term of the code in Ref.[18]. The linear instabilities of ion temperature gradient modes and kinetic ballooning modes are compared with those calculated in Ref.[16].

We examine the multi-scale-nonlinear interaction in a reversed shear plasma with $\beta = 1\%$. The equilibrium q profile is $q = \frac{rB_T}{RB_\theta} = 1.05 + 2(r/a)^2 + 1/(3r/a + 0.01)^4$, where R is the plasma major radius and a is the plasma minor radius. In the numerical calculation we set $\epsilon = a/R = 0.25$ and $\rho_i/a = 1/80$, where ρ_i is Larmor radius. The equilibrium profiles of density and temperature are $n_{eq} = 0.8 + 0.2\exp(-2(r/a)^2)$ and $T_{eq} = 0.55 + 0.45(1 - (r/a)^2)^2$ as drawn in Fig. 2. This equilibrium is unstable against the $(m, n) = (2, 1)$ double tearing mode because the q-profile has the $q = 2$ resonant surfaces[19]. The equilibrium is also unstable against the $6 < n < 22$ kinetic ballooning instabilities[20], i.e. micro-instabilities, as shown in Fig. 2. Notice that this tearing mode produces magnetic islands and that its growth rate is small compared to that of the micro-instability. A ballooning structure of the micro-instability appears in the bad curvature and positive shear region, as represented by the electric potential profile in Fig. 3. The double tearing mode spreads between two resonant surfaces of $q = 2$ at $r/a \approx 0.38$ and 0.69 as shown in Fig. 3.

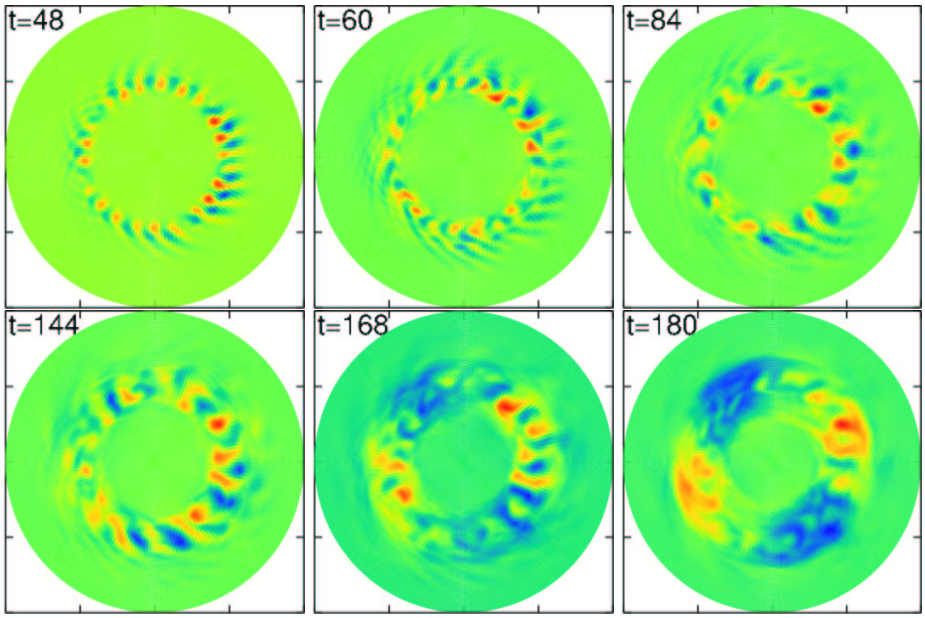

FIG. 4: *Time evolution of the electric potential on a poloidal section.*

3. Multi-scale nonlinear interactions

We now present nonlinear simulation results. We start the nonlinear simulation at $t = 0$ by taking the result of the linear calculation as the initial condition. We fix the background profiles of density and temperature, while we do not fix the q-profile. Figure 4 shows the electric potential on a poloidal section at $t = 48$, 60, 84, 144, 168, and 180, where the time is normalized by the ion thermal transit time. Figure 5 shows time evolution of the magnetic energy for each toroidal mode number n. The micro-instability induces zonal flow which has a stabilizing effect on the micro-instability by shearing radial structure of the instability. This is observed in Fig. 4 which presents the ballooning structure of the micro-instability is deformed by the flow at $t = 60$. Then the system reaches to a quasi-steady state after the turbulence balances with the zonal flow $t > 60$ in Fig. 5. In this quasi-steady state, the $m = 2$ double tearing mode appears and dominates the structure of electric potential at $t = 168$ and then the turbulence spreads over the plasma at $t = 180$. We examine these subsequent multi-scale nonlinear interactions in the following subsections in detail.

3.1. An equilibrium formed by a balance between micro-turbulence and zonal flow

We have strong nonlinear mode coupling represented by rapid growth of energy of high wave number at $t < 50$ in Fig. 5. A zonal flow with a $(m, n) = (0, 0)$ structure also appears through the nonlinear mode coupling as indicated by the n=0 line in Fig. 5. The spatial profile of zonal flow is shown in Fig. 6(a). The zonal flow is oscillating because of the geodesic acoustic mode which is a mode-coupling between (m,n)=(0,0) flow and (m,n)=(1,0) pressure perturbation. This zonal flow twists the radial structure of the micro-instability and suppresses the growth of the instability. When this suppression balances with the turbulence due to the micro-instability the

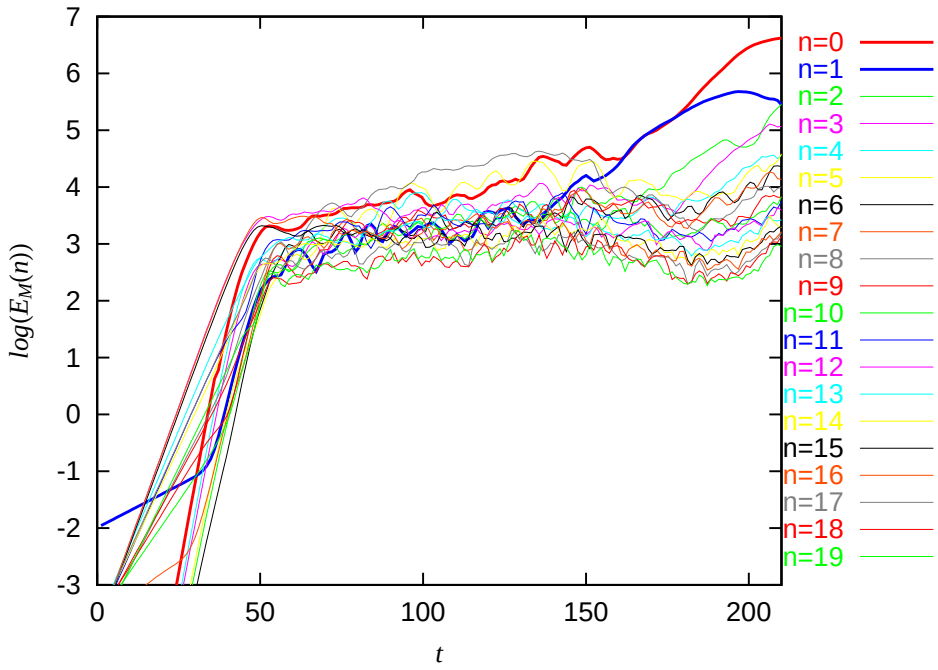

FIG. 5: *Time evolution of the magnetic energy for each toroidal mode* n.

system reaches to a steady state at $t = 60$. This steady state continues until macro-MHD, i.e. the tearing mode, appears at $t \approx 150$.

3.2. Nonlinear trigger of macro-MHD in the quasi-equilibrium

The energy of the $(m, n) = (2, 1)$ tearing mode, i.e. macro-MHD, grows nonlinearly from $t \approx 150$ and dominates at $t \approx 175$ in Fig. 5. The $m = 2$ structure appears correspondingly in the spatial profile of electric potential at $t = 168$ in Fig. 4. The energy of the $n = 0$ perturbation also increases in Fig. 5. This implies an alteration of magnetic field structure.

Let us investigate this $n = 1$ MHD mode in detail. Figure 7 shows the electric potential of the $n = 1$ mode at $t = 48$, 60, 84, 144, 168, and 180. When the system reaches to a steady state at $t = 60$, the $n = 1$ mode appears, however, the spatial distribution of the electric potential at $t = 60$ shown in Fig. 7 does not like the eigen function of double tearing mode in Fig. 3. This is because the $n = 1$ mode is caused by a nonlinear mode coupling not by the free energy of the equilibrium current density gradient. It seem that the radial structure is strongly twisted by a shear flow at $t = 60$ and 84 in Fig. 7. We believe that the zonal flow induced by the micro-instability has a stabilizing effect not only on the micro-turbulence but on the tearing mode by twisting their radial structure. On the other hand, when the $(m, n) = (2, 1)$ double tearing mode appears and dominates at $t \approx 170$ in Figs. 4 and 5, this twisting vanishes and the spatial distribution at $t = 168$ in Fig. 7 is similar to the eigen function of the double tearing mode in Fig. 3. A possible mechanism of this vanishing of shearing is the Maxwell stress acting on the poloidal flow. The stress is caused by the interaction between two magnetic islands chains[21], and it can weaken the shearing to lock the phase of two islands chains.

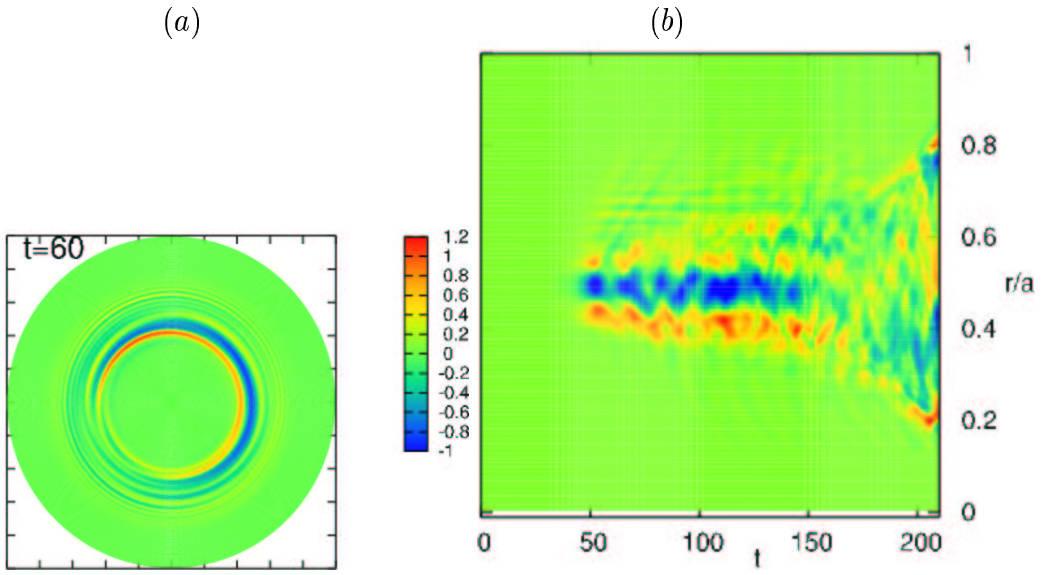

FIG. 6: *(a) Spatial profile of zonal flow on a poloidal section. (b) Time evolution of zonal flow profile along* $\theta = 0$ *axis on a poloidal section.*

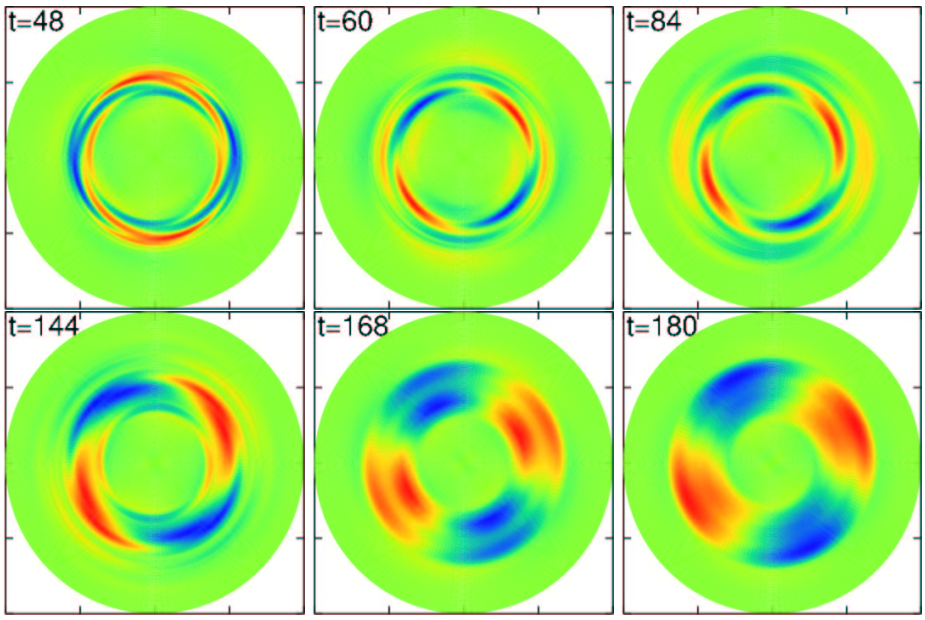

FIG. 7: *Time evolution of the electric potential of* $n = 1$ *mode on a poloidal section.*

3.3. Effect of tearing mode on micro-turbulence

The tearing mode affects the micro-turbulence because the tearing mode breaks the magnetic surfaces through magnetic reconnections. This violation spreads the micro-turbulence over the plasma after $t \approx 180$. The extension of the turbulent region is represented by the electric potential profiles at $t = 180$ in Fig. 4. This expansion is also observed in the evolution of zonal flow profile at $t > 160$ in Fig. 6(b). The violation also increases the energy of the turbulence as indicated by the traces with $n > 1$ at $t > 180$ in Fig. 5.

4. Summary and Discussion

We have found that the multi-scale nonlinear interaction gives rise to macro-MHD activity, which is a double tearing mode, after a quasi-steady equilibrium is formed by a balance between the micro-turbulence and zonal flow. This appearance of the tearing modes can explain the observation of macro-MHD activities in the experiment[1] that inherently includes turbulent fluctuation and zonal flow. We have also found this macro-MHD spreads the micro-turbulence due to the micro-instability over the plasma.

The mechanism of these interactions is as follows. At first, the toroidal-micro-instability dominates the linear evolution, and then zonal flow, which suppresses the instability, appears so that the system reaches to a quasi-steady state. The zonal flows also attempt to suppress the double tearing mode. However, the fluctuation due to the nonlinear-mode-coupling overcomes this suppression and produces the tearing mode in this quasi-steady state. This tearing mode breaks the magnetic surfaces, and thus the tearing mode spreads the turbulence over the plasma. The appearance of this non-ideal-macro-MHD activity due to nonlinear interactions can explain the evolution of $n = 1$ fluctuation observed before the disruption of reversed shear plasmas[1].

Here we discuss effects of turbulent initial conditions and flowing initial equilibrium in numerical simulations. We have obtained the quasi-steady state which is established by the balance between the micro-turbulence and the zonal flow at $60 < t < 140$ as shown in Fig. 5. We believe this quasi-steady state is the equilibrium including flow and turbulent fluctuation. Thus our numerical results involve these two effects and reveal a nonlinear destabilization of the macro-MHD from turbulent initial fluctuation in a quasi-equilibrium which is formed by a balance between the turbulence and zonal flow.

These multi-scale interactions are obtained by the numerical simulations with a reduced two-fluid equations. We will solve another reduced two-fluid equations from the full two-fluid equations in Ref.[22] and attempt to obtain general conclusion on the multi-scale nonlinear interactions.

Acknowledgments

The authors would like to thank Dr. N. Miyato at JAEA for useful discussions. They also thank Prof. Sudo for his encouragement. One of the authors A. I. is supported by the Japanese Ministry of Education, Culture, Sports, Science, and Technology, Grant No. 18760642.

References

[1] TAKEJI, S., *et al.*, Nuclear Fusion **42**, 5 (2002).
[2] TANAKA, K., *et al.*, Nuclear Fusion **46**, 110 (2006).
[3] DIAMOND, P. H., *et al.*, Plasma Physics and Controlled Fusion **47**, R35 (2005).
[4] HORTON, W., *et al.*, Review of Modern Physics **71**, 735 (1999).
[5] BISKAMP, D., *et al.*, Physics Letters **96A**, 25 (1983).
[6] BISKAMP, D., Plasma Physics and Controlled Fusion **26**, 311 (1984).
[7] DIAMOND, P. H., *et al.*, Phys. Fluids **27**, 1449 (1984).
[8] ITOH, S. -I., *et al.*, Plasma Physics and Controlled Fusion **46**, 123 (2004).
[9] YAGI, M., *et al.*, Nuclear Fusion **45**, 900 (2005).
[10] McDEVITT, C. J., *et al.*, Phys. Plasmas **13**, 032302 (2006).
[11] POUQUET, A., Journal of Fluid Mechanics **88**, 1 (1978).
[12] ISHIZAWA, A., *et al.*, Journal of the Physical Society of Japan **65**, 2033 (1996).
[13] HAZELTINE, R. D., *et al.*, Phys. Fluids **30**, 320 (1987).
[14] SCOTT, B., *et al.*, Phys. Plasmas **7**, 1845 (2000).
[15] GARBET, X., *et al.*, Phys. Plasmas **8**, 2793 (2001).
[16] MIYATO, N., *et al.*, Phys. Plasmas **11**, 5557 (2004).
[17] SATO, M., *et al.*, Phys. Plasmas **10**, 187 (2003).
[18] ICHIGUCHI, K., *et al.*, Nuclear Fusion **43**, 1101 (2003).
[19] ISHII, Y., *et al.*, Phys. Plasmas **7**, 4477 (2000).
[20] TANG, W. M., *et al.*, Nuclear Fusion **20**, 1439 (1980).
[21] FITZPATRICK, R., *et al.*, Phys. Fluids **B 3**, 644 (1991).
[22] RAMOS, J. J., Phys. Plasmas **12**, 052102 (2005).